Selsurtite, $(H_3O)_{12}Na_3(Ca_3Mn_3)(Na_2Fe)Zr_3\square Si[Si_{24}O_{69}(OH)_3](OH)Cl\cdot H_2O$, a new eudialyte-group mineral from the Lovozero alkaline massif, Kola Peninsula

NIKITA V. CHUKANOV[1,2]*, SERGEY M. AKSENOV[3,4], OLGA N. KAZHEVA[3], IGOR V. PEKOV[2], DMITRY A. VARLAMOV[5], MARINA F. VIGASINA[2], DMITRY I. BELAKOVSKIY[6], SVETLANA A. VOZCHIKOVA[1], SERGEY N. BRITVIN[7]

[1] Federal Research Center of Problems of Chemical Physics and Medicinal Chemistry, Russian Academy of Sciences, Chernogolovka, Moscow region, 142432 Russia

[2] Faculty of Geology, Moscow State University, Vorobievy Gory, 119991 Moscow, Russia

[3] Laboratory of Arctic Mineralogy and Material Sciences, Kola Science Centre, Russian Academy of Sciences, 14 Fersman str., Apatity 184209 Russia

[4] Geological Institute, Kola Science Centre, Russian Academy of Sciences, 14 Fersman str., Apatity 184209 Russia

[5] Institute of Experimental Mineralogy RAS, Chernogolovka, 142432 Russia

[6] Fersman Mineralogical Museum of the Russian Academy of Sciences, Leninsky Prospekt 18-2, 119071 Moscow, Russia

[7] Department of Crystallography, St Petersburg State University, Universitetskaya Nab. 7/9, 199034 St Petersburg, Russia

*E-mail: chukanov@icp.ac.ru

Running title: Selsurtite, a new mineral

Mineralogical Society

This is a 'preproof' accepted article for Mineralogical Magazine. This version may be subject to change during the production process.
DOI: 10.1180/mgm.2022.136

Abstract

The new eudialyte-group mineral selsurtite, ideally $(H_3O)_{12}Na_3(Ca_3Mn_3)(Na_2Fe)Zr_3\square Si[Si_{24}O_{69}(OH)_3](OH)Cl\cdot H_2O$, was discovered in metasomatic peralkaline rock from the Flora mountain, the northern spur of the Selsurt mountain, Lovozero alkaline massif, Kola Peninsula, Russia. The associated minerals are aegirine, albite and orthoclase, as well as accessory lorenzenite, calciomurmanite, natrolite, lamprophyllite, and sergevanite. Selsurtite occurs as brownish-red to reddish-orange, equant or flattened on (0001) crystals up to 2 mm across and elongate crystals up to 3 cm long. The main crystal forms are {0001}, {11-20}, and {10-11}. Selsurtite is brittle, with the Mohs' hardness of 5. No cleavage is observed. Parting is distinct on (001). *D*(meas) = 2.73(2), *D*(calc) = 2.722 g·cm^{-3}. Selsurtite is optically uniaxial, negative, with ω = 1.598(2) and ε = 1.595(2). The chemical composition is (wt.%, electron microprobe): Na_2O 6.48, K_2O 0.27, MgO 0.10, CaO 6.83, MnO 4.73, FeO 1.18, SrO 1.88, La_2O_3 0.57, Ce_2O_3 1.07, Pr_2O_3 0.20, Nd_2O_3 0.44, Al_2O_3 0.29, SiO_2 50.81, ZrO_2 13.50, HfO_2 0.45, TiO_2 0.61, Nb_2O_5 1.10, Cl 1.01, SO_3 0.29, H_2O 8.10, –O≡Cl –0.23, total 99.68. The empirical formula is $H_{25.94}Na_{6.03}K_{0.16}Mg_{0.07}Ca_{3.51}Sr_{0.52}Ce_{0.19}La_{0.10}Nd_{0.08}Pr_{0.03}Mn_{1.91}Fe_{0.47}Ti_{0.22}Zr_{3.16}Hf_{0.06}Nb_{0.24}Si_{24.40}$ $Al_{0.16}S_{0.10}Cl_{0.82}O_{79.13}$. The crystal structure was determined using single-crystal X-ray diffraction data and refined to *R* = 0.0484. Selsurtite is trigonal, space group *R*3, with *a* = 14.1475(7) Å, *c* = 30.3609(12) Å, *V* = 5262.65(7) Å^3, and *Z* = 3. Infrared and Raman spectra show that hydronium cations are involved in very strong hydrogen bonds and form Zundel- and Eigen-like complexes. The strongest lines of the powder X-ray diffraction pattern [*d,* Å (*I*, %) (*hkl*)] are: 11.38 (56) (101), 7.08 (59) (110), 5.69 (36) (202), 4.318 (72) (205), 3.793 (36) (303), 3.544 (72) (027, 220, 009), 2.970 (100) (315), 2.844 (100) (404). The mineral is named after the discovery locality.

Keywords: selsurtite; new mineral; eudialyte group; crystal structure; IR spectroscopy; Raman spectroscopy; peralkaline rock; Lovozero alkaline massif.

https://doi.org/10.1180/mgm.2022.136 Published online by Cambridge University Press

Introduction

The Selsurt mountain located in the north-eastern part of the well-known huge Lovozero alkaline complex, Kola Penisula, Russia is mainly composed of rocks belonging to the layered complex of urtites, foyaites, and lujavrites (Bussen and Sakharov, 1972). Various metasomatic assemblages occur at the contacts of the igneous alkaline rocks with metamorphic rocks on the northern spur of the Selsurt mountain.

The new Na-deficient eudialyte-group mineral selsurtite described in this paper is named after the discovery locality. The specimens with selsurtite were collected by one of the authors (NVC) in August, 1993.

Selsurtite is the 31st representative of the eudialyte group that includes trigonal minerals with the general formula $N1_3N2_3N3_3N4_3N5_3M1_6M2_{3-6}M3M4Z_3(Si_{24}O_{72})O'_{4-6}X1X2$ (Johnsen *et al.*, 2003) where *N*1–5 = Na, K, H_3O^+, Ca, Mn^{2+}, Sr, Ba, *REE*; *M*1 = Ca, Mn^{2+}, Fe^{2+}, *REE*, Na, Sr; *M*2 = Mn^{2+}, Fe^{2+}, Fe^{3+}, Na, Zr, Ta, Ti, K, H_3O^+; *M*3 and *M*4 = Si, S, Nb, Ti, W, Na; *Z* = Zr, Ti, Nb; O′ = O, OH, H_2O; *X*1 and *X*2 = F, Cl, H_2O, OH, CO_3, SO_4. The complex structures of these minerals are based on a heteropolyhedral framework composed of 9- and 3-membered rings of tetrahedra (Si_9O_{27}, Si_3O_9), 6-membered rings of octahedra $M1_6O_{24}$, ZO_6 octahedra and $^{[4–7]}M2O_n$ polyhedra. Additional *M*3 and *M*4 sites located at the centers of the Si_9O_{27} rings have 4- or 6-fold coordination. The framework hosts *N*1–*N*5 cations, *X*1–*X*2 anions and water molecules. In most eudialyte-group minerals, Na^+ dominates among *N* cations. The only exceptions are three hydronium-rich members of the eudialyte group, aqualite, $(H_3O)_8Na_4SrCa_6Zr_3Si_{26}O_{66}(OH)_9Cl$ (Khomyakov *et al.*, 2007), ilyukhinite, $(H_3O,Na)_{14}Ca_6Mn_2Zr_3Si_{26}O_{72}(OH)_2\cdot 3H_2O$ (Chukanov *et al.*, 2017), and selsurtite, $(H_3O)_{12}Na_3(Ca_3Mn_3)(Na_2Fe)Zr_3\square Si[Si_{24}O_{69}(OH)_3](OH)Cl\cdot H_2O$.

The new mineral and its name have been approved by the IMA CNMNC (IMA No. 2022-026). The holotype specimen is deposited in the collection of the Fersman Mineralogical Museum of the Russian Academy of Sciences, Moscow, Russia with the registration number 5843/1.

https://doi.org/10.1180/mgm.2022.136 Published online by Cambridge University Press

Experimental methods and data processing

In order to obtain IR absorption spectra, powdered samples were mixed with anhydrous KBr, pelletized, and analyzed using an ALPHA FTIR spectrometer (Bruker Optics) in the range of 360 – 3800 cm^{-1} at a resolution of 4 cm^{-1}. 16 scans were collected for each spectrum. The IR spectrum of an analogous pellet of pure KBr was used as a reference.

Raman spectrum of a randomly oriented samples were obtained using an EnSpectr R532 spectrometer based on an OLYMPUS CX 41 microscope coupled with a diode laser (λ = 532 nm) (Dept. of Mineralogy, Faculty of Geology, Moscow State University). The spectra were recorded at room temperature in the range from 100 to 4000 cm^{-1} with a diffraction grating (1800 gr mm^{-1}) and spectral resolution about 6 cm^{-1}. The output power of the laser beam was in the range from 5 to 13 mW. The diameter of the focal spot on the sample was 5 – 10 μm. The backscattered Raman signal was collected with a $40^{\times}$ objective; signal acquisition time for a single scan of the spectral range was 1 s, and the signal was averaged over 50 scans. Crystalline silicon was used as a standard.

Ten chemical analyses were carried out using a digital scanning electron microscope Tescan VEGA-II XMU equipped by energy-dispersive spectrometer (EDS) INCA Energy 450 with semiconducting Si (Li) detector Link INCA Energy at an accelerating voltage of 20 kV, electron current of 190 pA and electron beam diameter of 160–180 nm. Attempts to use WDS mode, with a higher beam current, were unsuccessul because of instability of the mineral under electron beam due to partial dehydration and migration of Na. This phenomenon is typical for high-hydrous sodium minerals with microporous structures.

A good agreement was observed between compositional data obtained under these standard conditions and those obtained under more “mild” conditions (with a current lowered to 90 – 100 pA and electron beam defocused to an area of 30 × 30 μm).

https://doi.org/10.1180/mgm.2022.136 Published online by Cambridge University Press

The *L*-lines of Ta are not observed in the spectrum, which indicates the absence of detectable amounts of tantalum in selsurtite. Taking into account overlapping of the Sr*L*α and Si*K*α peaks, the SrO content has been measured by the WDS-mode analysis using the Sr*L*α1 line, at an accelerating voltage of 20 kV and a current of 20 nA. The size of an electronic "spot" on a surface of a sample was 300 to 320 nm.

The H_2O content was determined by means of a modified Penfield method. The CO_2 content was not determined because characteristic bands of carbonate groups (in the range of 1350 – 1550 cm^{-1}) are not observed in the IR spectrum of selsurtite. Analytical data are given in Table 1. Contents of other elements with atomic numbers >8 are below detection limits.

Powder X-ray diffraction data were collected using a Rigaku R-AXIS Rapid II diffractometer (image plate), Co*K*α, 40 kV, 15 mA, rotating anode with the microfocus optics, Debye-Scherrer geometry, d = 127.4 mm, exposure 15 min. The raw powder XRD data were collected using program suite designed by Britvin *et al.* (2017). Calculated intensities were obtained by means of STOE WinXPOW v. 2.08 program suite based on the atomic coordinates and unit-cell parameters.

The single-crystal X-ray diffraction data for selsurtite were collected at room temperature by means of a Rigaku XtaLAB Synergy diffractometer with graphite monochromatized MoK_α radiation and a Hybrid Pixel Array detector using the ω scanning mode. A semi-empirical absorption correction based on intensities of equivalent reflections was applied, and the data were corrected for the Lorentz, polarization and background effects (Oxford Diffraction, 2009). The analysis of systematic absences of reflections shows *R*-centering, common for eudialyte-group minerals. Space group *R*3 was chosen based on cation ordering and lowering of the symmetry like other Ca-deficient (with less than 4.5 Ca *apfu*) members of the oneillite subgroup. The experimental details of the data collection and refinement results are listed in Table 1.

Results

https://doi.org/10.1180/mgm.2022.136 Published online by Cambridge University Press

Occurrence, General Appearance and Physical Properties

In the holotype specimen (Figures 1a, 2), selsurtite is a rock-forming mineral which constitutes about 15 vol.% of a metasomatic fenite-like peralkaline rock mainly composed of aegirine, albite and orthoclase. Platy crystals of orthoclase (up to 0.5 × 2 × 2 mm) are embedded in a fine-grained aggregate composed of aegirine and albite. Subordinate minerals are lorenzenite, calciomurmanite, natrolite, Mn- and Ba-rich lamprophyllite, and sergevanite. Sergevanite occurs as small relics in some selsurtite crystals (Figure 2b). Calciomurmanite forms pseudomorphs after platy lomonosovite crystals (up to 2×2×0.3 cm^3) embedded in the rock. The latest-stage mineral is saponite which forms pseudomorphs after grains of an unidentified mineral up to 1 mm across.

Selsurtite holotype occurs as equant or slightly flattened on (001) crystals up to 2 mm across (Figure 1a). In some parts of the rock, larger prismatic and rhombohedral selsurtite crystals up to 3 cm long occur together with crystals of lorenzenite and/or calciomurmanite reaching several centimeters across (Figure 1a). The main crystal forms are the pinacoid {0001}, the hexagonal prism {11-20} and the rhombohedron {10-11}.

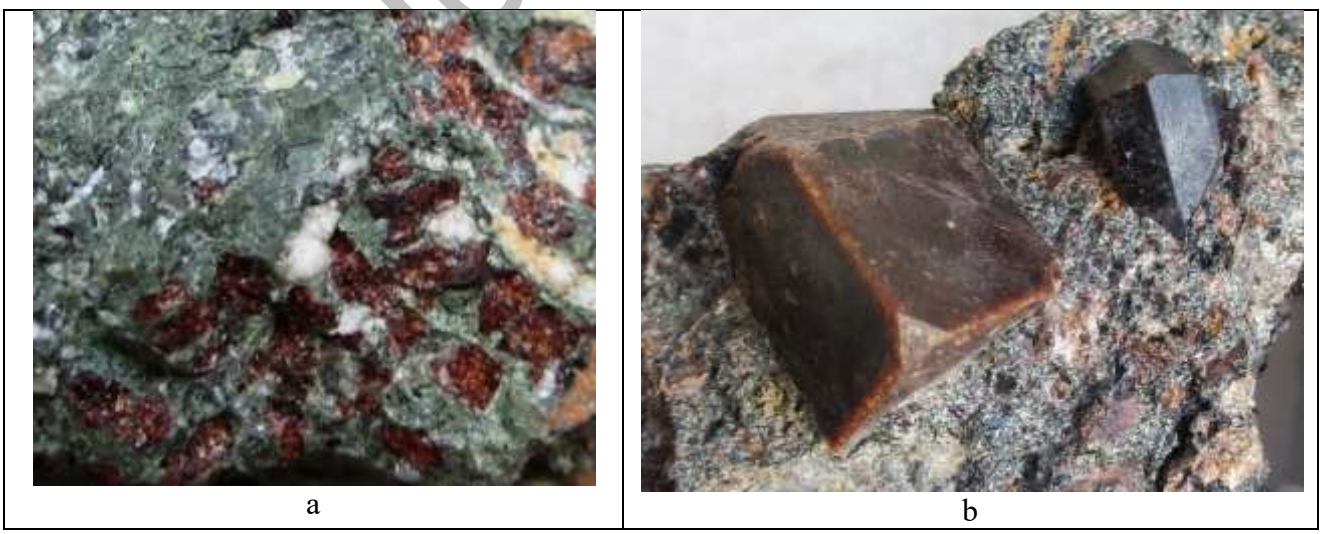

a b

Fig. 1. A fragment of the holotype specimen (registration number 5843/1 in the Fersman mineralogical museum) with red to reddish-orange selsurtite grains emnedded in the aegirine-feldspar rock (a) and selsurtite crystal (brownish-red on the left) in association with lorenzenite (dark brown on the right) (b). The FOV widths are 15 mm (a) and 4 cm (b).

https://doi.org/10.1180/mgm.2022.136 Published online by Cambridge University Press

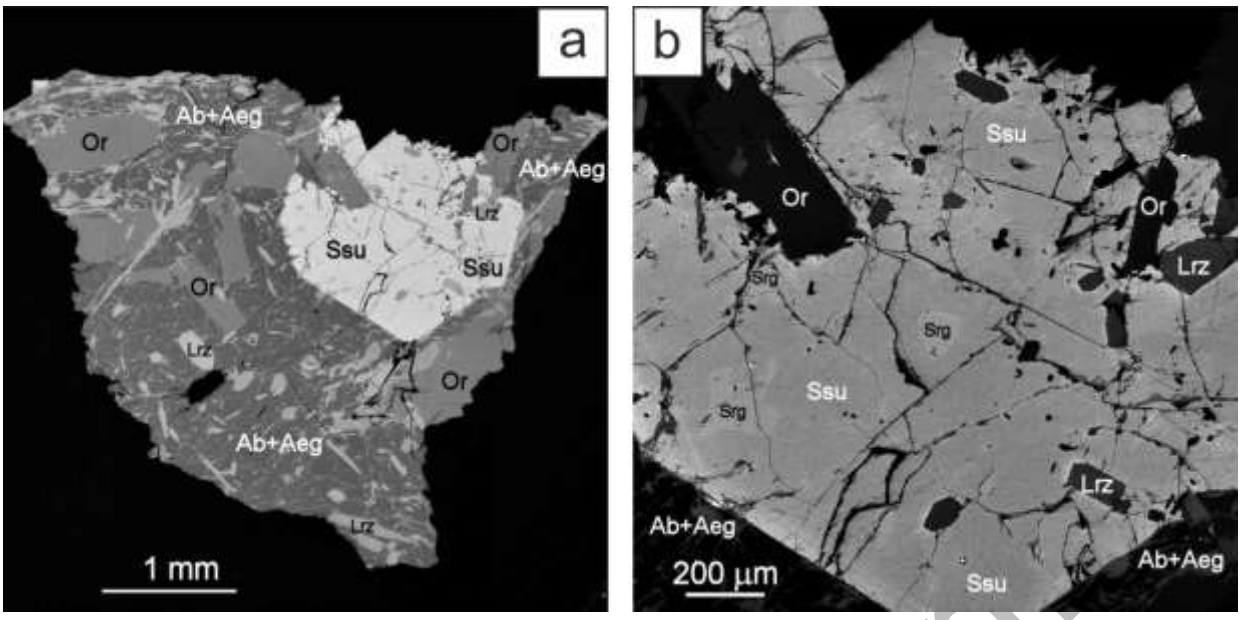

Fig. 2. SEM (BSE) image of a polished section of a fragment of selsurtite (Ssu) holotype specimen (specimen No. 5843/1 from the Fersman mineralogical museum) in a rock composed of aegirine (Aeg), orthoclase (Or) and albite (Ab) with accessory lorenzenite (Lrz) (a) and enlarged fragment of this image showing relics of sergevanite (Sgv) with the empirical formula $Na_{9.47}(H_3O)_xK_{0.16}Sr_{0.47}(Ca_{3.48}Mn_{2.01}Fe_{0.32}Ln_{0.19})(Na_{2.05}Fe_{0.56}Zr_{0.39})(Zr_{2.84}Ti_{0.09}Hf_{0.07})(Si_{25.58}Nb_{0.42})Cl_{1.00}(SO_4)_{0.04}(O,OH)_y{\cdot}nH_2O$ in the selsurtite crystal (b).

The color of selsurtite is brownish-red to reddish-orange. Some small transparent grains demonstrate strong dichroism: cherry red along (001) and orange across (001). The streak of the mineral is white.

Selsurtite is brittle, with the Mohs' hardness of 5. No cleavage is observed. Parting is distinct on (0001). The fracture is uneven. Density measured by flotation in heavy liquids (mixtures of methylene iodide and heptane) is equal to 2.73(2) $g{\cdot}cm^{-3}$. Density calculated using the empirical formula and unit-cell volume refined from single-crystal XRD data equals to 2.722 $g{\cdot}cm^{-3}$.

The new mineral is optically uniaxial, negative, with $\omega = 1.598(2)$ and $\varepsilon = 1.595(2)$ ($\lambda = 589$ nm). Under the microscope, selsurtite is pleochroic in thick grains (O = pinkish, E = pale yellow-pinkish). The absorption scheme is: $O > E$.

Infrared spectroscopy

https://doi.org/10.1180/mgm.2022.136 Published online by Cambridge University Press

Absorption bands in the IR spectrum of selsurtite (curve *a* in Figure3) and their assignments are (cm^{-1}; s – strong band, w – weak band, sh – shoulder): 3520sh, 3417, 3260sh (O–H stretching vibrations), 1639w (H–O–H bending vibrations), 1150sh (asymmetric stretching vibrations of SO_4 tetrahedra), 1003s, 981s, 935sh (Si–O stretching vibrations), 741 (mixed vibrations of rings of SiO_4 tetrahedra – "ring band"), 667w (mixed vibrations of rings of SiO_4 tetrahedra combined with Nb–O stretching vibrations), 520sh [^{IV}(Zr,Fe)–O stretching vibrations], 473s, 451s (lattice mode involving predominantly bending vibrations of rings of SiO_4 tetrahedra), 370 (lattice modes involving ^{VI}(Ca,Mn^{2+})–O stretching vibrations). The shoulder at 1300 cm^{-1} may correspond to isolated proton at the *N*5 site (Chukanov and Chervonnyi, 2016). The assignment of the IR bands was made based on the analysis of IR spectra of several tens structurally investigated eudialyte-group minerals, in accordance with Rastsvetaeva *et al*. (2012).

The IR spectrum of selsurtite differs from that of its sodium analogue sergevanite (curve *b* in Figure 3) in higher intensities of the bands of O–H stretching and H–O–H bending vibrations. A very low intensity of the band at 520 cm^{-1} observed as a shoulder in the IR spectrum of selsurtite reflects a low content of transitional elements at the *M*2 site which is in agreement with the structural data (see below).

https://doi.org/10.1180/mgm.2022.136 Published online by Cambridge University Press

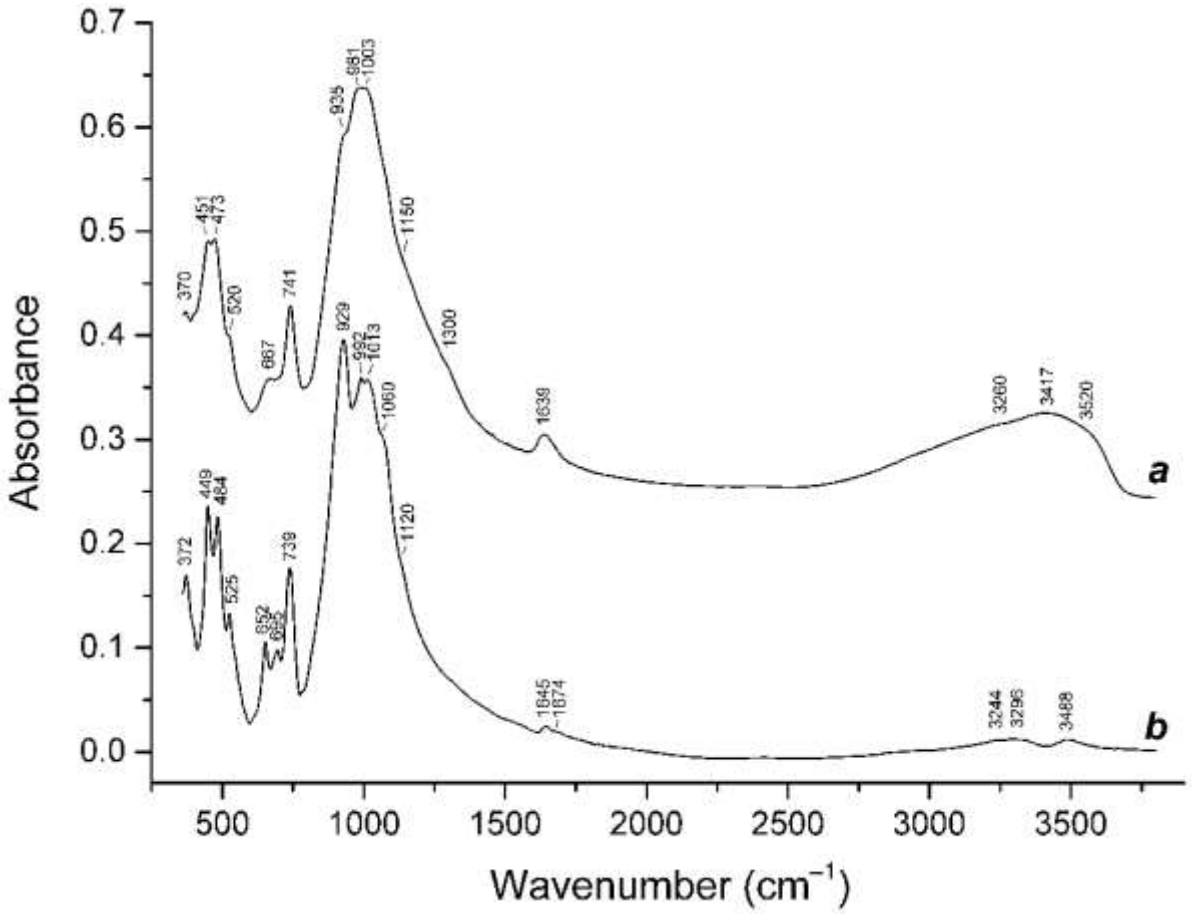

Fig. 3. Powder infrared absorption spectra of (*a*) selsurtite and (*b*) sergevanite holotype sample with the crystal-chemical formula $^{N1\text{-}4}(Na_{10.5}K_{0.9}REE_{0.6})$ $^{N5}[(H_3O,H_2O)_{2.25}Na_{0.75}]$ $^{M1_1}Ca_3$ $^{M1_2}(Mn_{1.8}Ca_{1.2})$ $^{M2}(Na_{2.4}Fe^{2+}_{0.6})$ $^{M3}(Si_{0.5}Ti_{0.45}Nb_{0.05})$ ^{M4}Si $^{Z}(Zr_{2.7}Nb_{0.3})$ $[Si_3O_9]_2$ $[Si_9O_{27}]_2$ $(OH)_3$ $(SO_4)_{0.3}$ $^{X1}[(H_2O)_{0.8}Cl_{0.2}]$. The spectra are offset for comparison.

Raman spectroscopy

A specific feature of the Raman spectrum of selsurtite (Fig. 4), as well as other hydronium-bearing eudialyte-group minerals (the curves *a* and *b* in Fig. 5) is a series of bands in the range of 1070 – 2900 cm^{-1} corresponding to strong hydrogen bonds formed by hydronium cations in different local situations including Zundel- and Eigen-like ones with short O···O distances of ~2.4 and ~2.6 Å (see Discussion section for details). These bands are absent in the Raman spectrum of eudialyte which does not contain H_3O^+ cations (the curve *c* in Fig. 5).

The assignment of other bands in the Raman spectrum of selsurtite is as follows.

https://doi.org/10.1180/mgm.2022.136 Published online by Cambridge University Press

3455 and 3550 cm^{-1} – O–H stretching vibrations of H_2O molecules and OH groups.

The range 900 – 1100 cm^{-1} – Si–O stretching modes (maybe, except the band at 1073 cm^{-1} which may correspond to hydrated proton complex having Zundel-like configuration: see Authors' remarks).

792 cm^{-1} – mixed vibrations of rings of SiO_4 tetrahedra.

650 and 691 cm^{-1} – mixed vibrations of rings of SiO_4 tetrahedra combined with Nb–O stretching vibrations.

564 cm^{-1} – ^{IV}(Zr,Fe)–O stretching vibrations.

≤ 410 cm^{-1} – lattice modes.

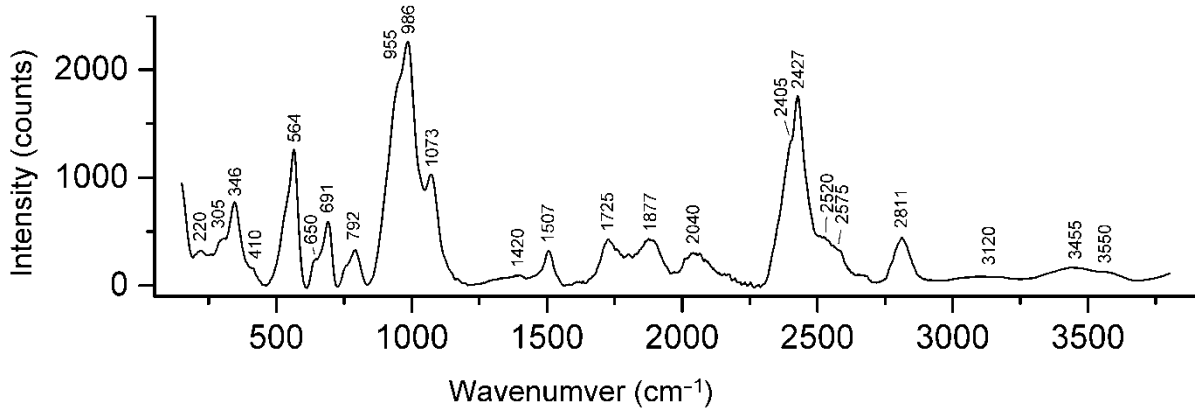

Fig. 4. Raman spectrum of selsurtite.

https://doi.org/10.1180/mgm.2022.136 Published online by Cambridge University Press

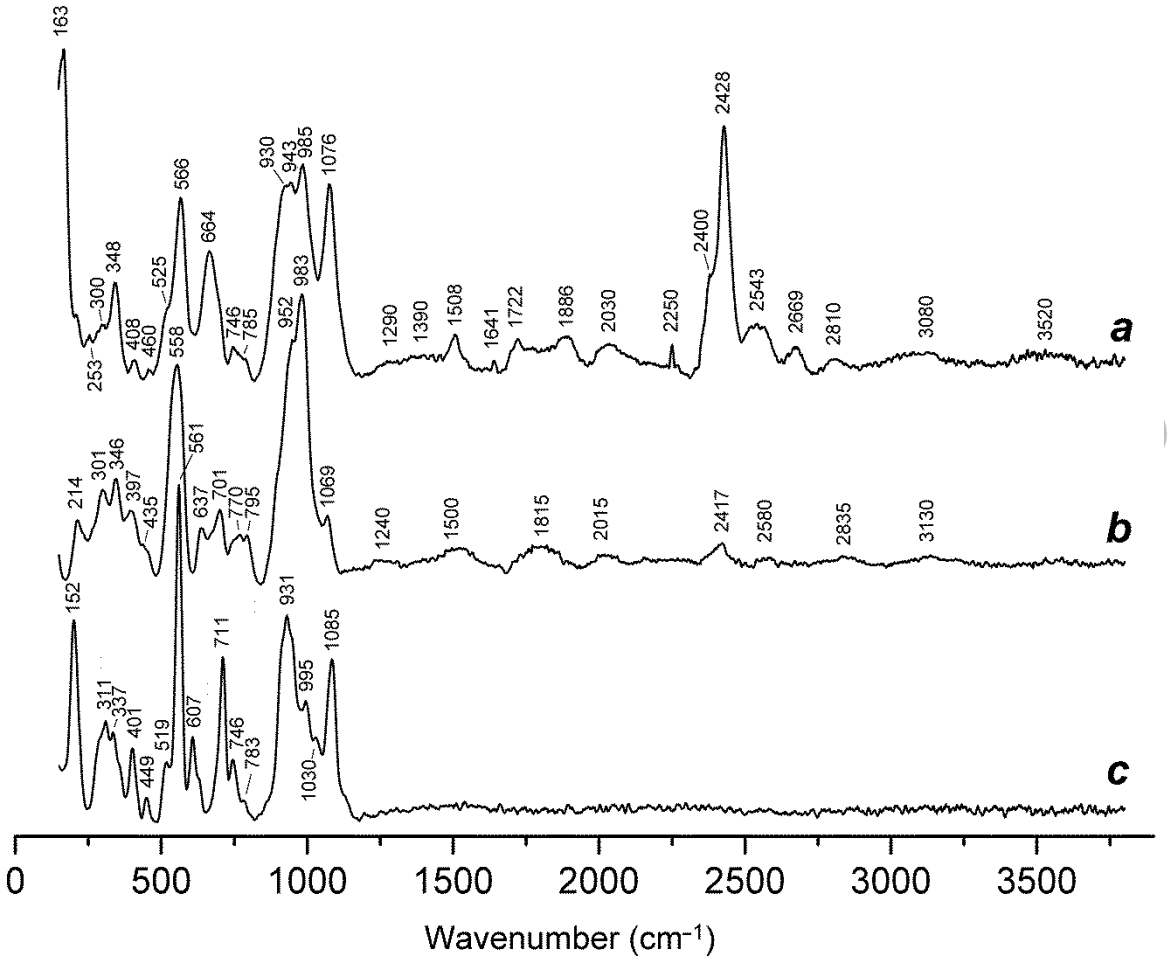

Fig. 5. Raman spectra of (*a*) potassium analogue of aqualite $(H_3O)_8Na_5K_2Zr_3Ca_6[Si_{24}O_{69}(OH)_3][Si_2]Mn(OH)_2Cl\cdot 2H_2O$ from the Kovdor ultrabasic-alkaline-carbonatite complex, Kola Peninsula, Russia (Rastsvetaeva *et al*., 2022), (*b*) "potassium-oxonium eudialyte" with the empirical formula $(H_3O)_x(Na_{3.3}K_{2.5}Sr_{0.6})Ca_{6.4}Mn_{0.15}Fe_{1.3}Zr_{2.8}Ti_{0.2}Nb_{0.15}Si_{25.85}Cl_{1.7}(O,OH)_x\cdot nH_2O$ ($x \approx 8$) from the Kukisvumchorr mountain, Khibiny alkaline massif, Kola Peninsula (Rastsvetaeva *et al*., 2012), and (*c*) common accessory eudialyte $Na_{15}Ca_6Fe^{2+}{}_3Zr_3Si_{26}O_{72}(O,OH,H_2O)_3Cl_2$ from the Alluaiv mountain, Lovozero alkaline massif, Kola Peninsula.

Chemical Data

Analytical data are given in Table 2. The empirical formula (based on 24.56 Si+Al *apfu*, $Z = 3$, in accordance with structural data) is $H_{25.94}Na_{6.03}K_{0.16}Mg_{0.07}Ca_{3.51}Sr_{0.52}Ce_{0.19}La_{0.10}Nd_{0.08}Pr_{0.03}Mn_{1.91}Fe_{0.47}Ti_{0.22}Zr_{3.16}Hf_{0.06}Nb_{0.24}Si_{24.40}Al_{0.16}S_{0.10}Cl_{0.82}O_{79.13}$. Taking into account structural data (see below), the simplified formula can be written as follows: $(H_3O,Na,\square)_{15}[(Mn,Ca)_3(Ca,Mn)_3]$

https://doi.org/10.1180/mgm.2022.136 Published online by Cambridge University Press

$(Na_2(Fe,Zr)](□,Nb,Si)(Si,Ti,□)(Si_3O_9)_2[Si_9(O,OH)_{27}]_2(OH)Cl \cdot H_2O$. The ideal formula is $(H_3O)_{12}Na_3(Mn_3Ca_3)(Na_2Fe)Zr_3□Si[Si_{24}O_{69}(OH)_3](OH)Cl \cdot H_2O$

The Gladstone-Dale compatibility index $1 - (K_p/K_c)$ (Mandarino, 1981) is equal to –0.011 (rated as superior) with the density calculated using the empirical formula and unit-cell parameters refined from the single-crystal X-ray diffraction data.

X-ray Diffraction and Crystal Structure

Powder X-ray diffraction data of selsurtite are given in Table 3. The unit-cell parameters refined from the powder data are: a = 14.162(2) Å, c = 30.41(1) Å, and V = 5282(4) Å^3.

The crystal structure was solved and refined based on 2752 independent reflections with $I > 3\sigma(I)$ using the program package JANA2006 (Petříček *et al.*, 2006). Extra-framework sites, including split and partially occupied ones, were located in a difference electron-density map. Atomic scattering factors for neutral atoms, together with anomalous dispersion corrections, were taken from *International Tables for Crystallography* (Prince *et al.*, 2004). Illustrations were produced with the JANA2006 program package in combination with the program DIAMOND (Brandenburg and Putz, 2005). Because of the complex chemical composition, the cation distribution on the structural sites was proposed taking into account site-scattering factors, interatomic distances and ionic radii of the cations. At the first step, the number of electrons associated with the atoms at the sites (e_{calc}) was determined. At the second step, for each value of e_{calc}, the most suitable ratio between the atoms with the closest final refined amount of electrons (e_{ref}) was selected and atoms coordinates and ADPs were refined.

The final refinement cycles converged to R_1 = 4.84%, wR_2 = 7.15%, and GOF = 1.14. The highest peak and deepest minimum in the final residual electron density were 1.14 e Å^{-3} and −1.11 e Å^{-3}, respectively. Table 4 lists the fractional atomic coordinates, site multiplicities, atomic displacement parameters and site occupancies. Selected interatomic distances are given in Table 5.

https://doi.org/10.1180/mgm.2022.136 Published online by Cambridge University Press

CSD 2157470 contains the supplementary crystallographic data for this paper. These data can be obtained free of charge *via* www.ccdc.cam.ac.uk/data_request/cif, by emailing data_request@ccdc.cam.ac.uk, or by contacting the Cambridge Crystallographic Data Center, 12 Union Road, Cambridge CB2 1EZ, UK; fax: +441223336033.

Discussion

Crystal structure

Selsurtite is isostructural with other 12-layered members of the oneillite-type (with the space group *R*3) reprersentatives of the eudialyte group. Based on the refined site-scattering factors, the crystal chemical formula of selsurtite can be written as follows (Z = 3): $\{^{N1}[(H_3O)_{2.40}Na_{0.60}]$ $^{N2}[(H_3O)_{2.1}Na_{0.9}]$ $^{N3}[Na_{1.8}(H_3O)_{0.84}Sr_{0.36}]$ $^{N4}[(H_3O)_{0.90}Na_{0.70}K_{0.18}]$ $^{N5}H_x\}$ $\{^{Z}(Zr_{2.93}Hf_{0.07})$ $^{M1(1)}(Mn_{1.82}Ca_{0.98}Ce_{0.2})$ $^{M1(2)}(Ca_{2.7}Mn_{0.19}Ce_{0.11})$ $^{M2}[Na_{2.12}Fe_{0.50}Zr_{0.38}(H_2O)_{1.28}]$ $^{M3}[\square_{0.44}(Nb(OH)_3)_{0.3}(SiOH)_{0.26}]$ $^{M4}[(SiOH)_{0.30}(Ti(OH)_3)_{0.23}\square_{0.47}]$ $[Si_3O_9]_2$ $[Si_9O_{25.59}(OH)_{1.41}]$ $[Si_9O_{25.68}(OH)_{1.32}]$ $^{X1}(Cl_{0.81}S_{0.12}F_{0.07})$ $^{X2}(H_2O)_{0.16}$.

The main structural features of selsurtite distinguishing it from other eudialyte-group minerals are:

(i) Cation ordering within the six-membered ring of octahedra resulting in a lowering of symmetry. The six-membered ring is formed by $M1(1)O_6$- and $M1(2)O_6$-octahedra with different occupancies (Fig. 6). The $M1(1)O_6$-octahedron is predominantly occupied by manganese (1.82 *apfu*), while the $M1(2)O_6$-octahedron is predominantly occupied by calcium (2.7 *apfu*).

(ii) The statistical predominance of sodium (2.12 *apfu*) at the *M*2 site.

(iii) The predominance of vacancies over $NbO_3(OH)_3$ octahedra and $SiO_3(OH)$ tetrahedra at the *M*3 site.

(iv) The predominance of tetravalent atoms (with Si > Ti) at the *M*4 site.

https://doi.org/10.1180/mgm.2022.136 Published online by Cambridge University Press

The predominance of hydronium at the extra-framework *N* sites.

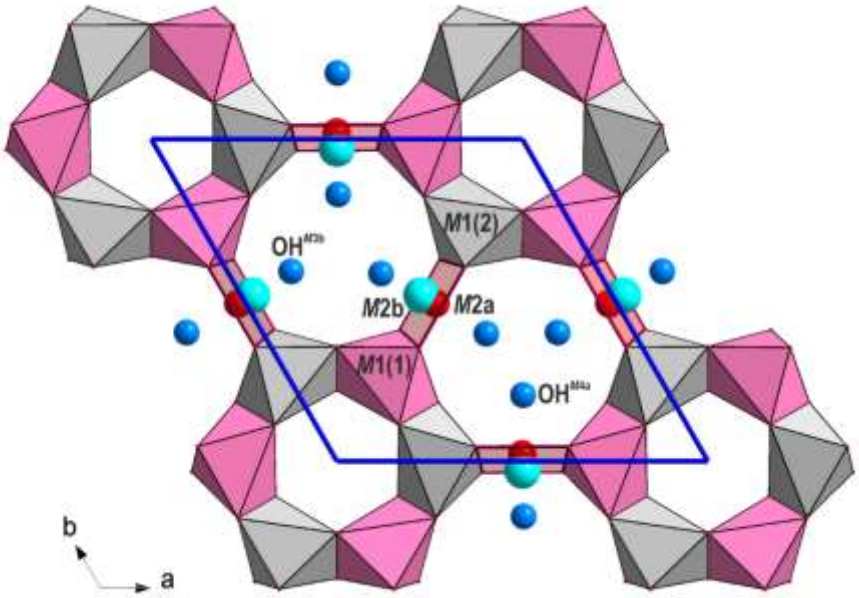

Fig. 6. The distribution of Na and Zr over the *M*2-sites in the crystal structure of selsurtite.

Raman spectroscopy of hydronium and hydrated proton complexes

Numerous *ab initio* quantum-chemical calculations of hydronium and other hydrated proton complexes, including Zundel ($H_5O_2^+$) and Eigen ($H_3O^+ \cdot 3H_2O$) cations have shown that these clusters are characterized by variable configurations and strong hydrogen bonds with the O···O distances in the range of 2.38 – 2.8 Å (Vyas, 1978; Komatsuzaki and Ohmine, 1994; Corongiu, 1995; Kim *et al*., 2002; Sobolewski and Domcke, 2002a,b; Asmis *et al*., 2003; Christie, 2004; Headrick *et al*., 2004; Laria *et al*., 2004; Asthagiri *et al*., 2005; Ortega *et al*, 2005; Paddison *et al*., 2005; Vener and Librovich, 2009; Biswas et al., 2017; Carpenter, 2020). Calculated wavenumbers of vibrational modes corresponding to the hydrated proton complexes are in the range of 1070 – 3000 cm^{-1}.

There is a negative correlation between the frequency of O–H stretching vibrations and O···O distance between O atom of OH group and O atom – acceptor of hydrogen bond (McClellan

https://doi.org/10.1180/mgm.2022.136 Published online by Cambridge University Press

and Pimentel, 1960; see Fig. 7). This correlation is nearly linear in the range of the O···O distances from 2.4 to 2.8 Å and significantly deviates from the linearity for weaker hydrogen bonds.

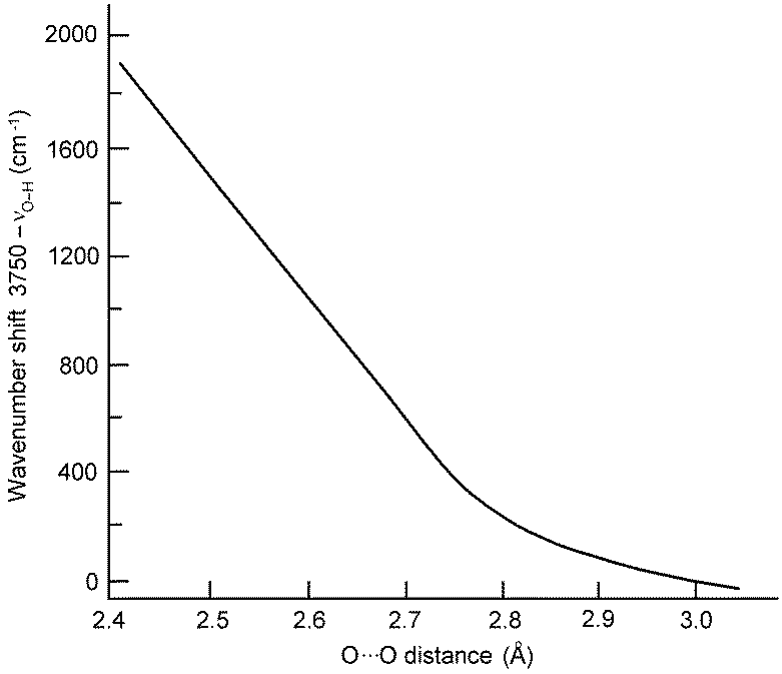

Fig. 7. The dependence of the wavenumber shift of O–H stretching vibrations relative to the value of 3750 cm^{-1} (accepted for non-bonded OH group) on the O···O distances for hydrogen bonds in crystals drawn using data from McClellan & Pimentel (1960).

The following empirical correlations between O–H stretching frequencies in IR spectra of minerals and O···O and H···O distances (obtained from structural data) were established by E. Libowitzky (1999):

$$\nu\ (\mathrm{cm}^{-1}) = 3592 - 304\cdot10^{9}\cdot\exp[-d(\mathrm{O}\cdots\mathrm{O})/0.1321] \quad (1)$$

$$\nu\ (\mathrm{cm}^{-1}) = 3632 - 1.79\cdot10^{6}\cdot\exp[-d(\mathrm{H}\cdots\mathrm{O})/0.2146] \quad (2)$$

Actually, the equations (1) and (2) are a very rough approximation and have a restricted applicability. In particular, above 3500 cm^{-1} substantial deviations from the correlations (1) and (2) are common because O–H stretching frequencies depend not only on O···O and H···O distances, but also on the nature of cations coordinating O–H groups and H_2O molecules, as well as on the O–H···O angle, and the influence of these factors becomes most evident in the case of weak hydrogen bonds. The equations (1) and (2) predict that maximum possible values of O–H stretching

https://doi.org/10.1180/mgm.2022.136 Published online by Cambridge University Press

frequencies for minerals are 3592 and 3632 cm^{-1}, respectively, but in many minerals including for magnesium serpentines, brucite, kaolinite, amphiboles *etc*. observed frequencies are much higher and can exceed 3700 cm^{-1}. However, these correlations can be used for semiquantitative estimations, at least for relatively strong hydrogen bonds. The proposed assignment of Raman bands of O–H stretching vibrations involving H_3O^+ groups are given in Table 6.

Origin of selsurtite

Despite selsurtite is a Na-deficient member of the eudialyte group, its crystal structure is characterized by the presence of the Na-dominant *M*2 site. Except selsurtite, only two 12-layer eudialyte-group minerals, raslakite, $^{N1\text{-}N5}Na_{15}{}^{M1}[Ca_3Fe_3]^{M2}(Na_2Zr)^{Z}Zr_3{}^{M3,M4}[(Si,Nb)Si](Si_{24}O_{72})(OH,H_2O,O)_4(Cl,OH)$ (Chukanov *et al*., 2003), and sergevanite, $^{N1\text{-}N5}(Na,H_3O)_{15}{}^{M1}(Ca_3Mn^{2+}{}_3)^{M2}(Na_2Fe^{2+})^{Z}Zr_3{}^{M3,M4}[Si(Si,Ti)][Si_{24}O_{72}](OH,H_2O,SO_4)_5$ (Chukanov et *al.*, 2020) have a Na-dominant *M*2 site. These minerals originate from highly alkaline, hyperagpaitic rocks. In other 12-layer eudialyte-group minerals, the *M*2 site is predominantly occupied by Fe^{2+}, Fe^{3+} or Mn^{2+}, or is vacant. The presence of sergevanite relics in some selsurtite crystals (Fig. 2) indicates that selsurtite could be formed as a result of leaching of sodium, protonation and hydration of sergevanite that initially crystallized under highly alkaline conditions. This assumption is in agreement with the association of selsurtite with calciomurmanite forming pseudomorphs after lomonosovite, a mineral considered as a marker of peralkaline conditions. Like the evolution series sergevanite → selsurtite, the evolution series lomonosovite $Na_{10}Ti_4(Si_2O_7)_2(PO_4)_2O_4$ → calciomurmanite $(Na,\square)_2Ca(Ti,Mg,Nb)_4[Si_2O_7]_2O_2(OH,O)_2(H_2O)_4$ (Lykova *et al*., 2016) is characterized by a significant leaching of Na^+ and hydration.

Comparative data for selsurtite and other Na-deficient, hydronium-rich eudialyte-group minerals are given in Table 7.

https://doi.org/10.1180/mgm.2022.136 Published online by Cambridge University Press

Acknowledgements

The authors are grateful to reviewers for the useful discussion. A major part of this work, including chemical analyses, infrared sperctroscopy, and identification of associated minerals was carried-out in accordance with the state task of Russian Federation, state registration number AAAA-A19-119092390076-7. The authors thank the X-ray Diffraction Centre of Saint-Petersburg State University for instrumental and computational resources.

Conflict of interest. The authors declare no conflict of interest.

Supplementary material. To view supplementary material for this article, please visit https://doi.org/...

https://doi.org/10.1180/mgm.2022.136 Published online by Cambridge University Press

References

Asmis K.R., Pivonka N.L., Santambrogio G., Brümmer M., Kaposta C., Neumark D.M., Wöste L. (2003) The gasphase infrared spectrum of the protonated water dimer. *Science*, **299**, 1375–1381.

Asthagiri D., Pratt L.R., Kress J.D. (2005) *Ab initio* molecular dynamics and quasichemical study of $H^+(aq)$. *Proceedings of the National Academy of Sciences of the United States of America*, **102**, 6704-6708. www.pnas.org_cgi_doi_10.1073_pnas.0408071102

Biswas R., Carpenter W., Fournier J.A., Voth G.A., Tokmakoff A. (2017) IR spectral assignments for the hydrated excess proton in liquid water. *Journal of Chemical Physics*, **146**, paper 154507. https://doi.org/10.1063/1.4980121

Brandenburg K. and Putz H. (2005): *DIAMOND* Version 3. Crystal Impact GbR. Bonn, Germany.

Britvin S.N., Dolivo-Dobrovolsky D.V., Krzhizhanovskaya M.G. (2017) Software for processing the X-ray powder diffraction data obtained from the curved image plate detector of Rigaku RAXIS Rapid II diffractometer. *Zapiski Rossiiskogo Mineralogicheskogo Obshchestva* (*Proceedings of the Russian Mineralogical Society*), **146**(3), 104–107 (in Russian).

Bussen I.V. and Sakharov A.S. (1972) Petrology of the Lovozero Alkaline Massif. Nauka Publishing, Leningrad, 296 pp. (in Russian).

Carpenter W.B. (2020) Aqueous proton structures and dynamics observed with nonlinear infrared spectroscopy. Ph. D. dissertation, the University of Chicago, 346 pp.

Christie R.A. (2004) *Theoretical Studies of Hydrogen-Bonded Clusters*. Ph.D. Thesis, University of Pittsburgh, 135 pp.

Chukanov N.V., Pekov I.V., Zadov A.E., Korovushkin V.V., Ekimenkova I.A., Rastsvetaeva R.K. (2003) Ikranite, $(Na,H_3O)_{15}(Ca,Mn,REE)_6Fe^{3+}{}_2Zr_3(\square,Zr)(\square,Si)Si_{24}O_{66}(O,OH)_6Cl{\cdot}nH_2O$, and raslakite, $Na_{15}Ca_3Fe_3(Na,Zr)_3Zr_3(Si,Nb)(Si_{25}O_{73})(OH,H_2O)_3(Cl,OH)$, new eudialyte-group minerals from the Lovizero massif. *Zapiski Rossiiskogo Mineralogicheskogo Obshchestva* (*Proceedings of the Russian Mineralogical Society*), **132**(5), 22–33 (in Russian).

https://doi.org/10.1180/mgm.2022.136 Published online by Cambridge University Press

Chukanov N.V. and Chervonnyi A.D. (2016) *Infrared Spectroscopy of Minerals and Related Compounds*. Springer: Cham–Heidelberg–Dordrecht–New York–London, 1109 pp. DOI: 10.1007/978-3-319-25349-7.

Chukanov N.V., Rastsvetaeva R.K., Rozenberg K.A., Aksenov S.M., Pekov I.V., Belakovsky D.I., Kristiansen R., Van K.V. (2017) Ilyukhinite, $(H_3O,Na)_{14}Ca_6Mn_2Zr_3Si_{26}O_{72}(OH)_2\cdot 3H_2O$, a new mineral of the eudialyte group. *Geology of Ore Deposits*, **59**, 592–600. DOI: 10.1134/S1075701517070030.

Chukanov N.V., Aksenov S.M., Pekov I.V., Belakovskiy D.I., Vozchikova S.A., Britvin S.N. (2020) Sergevanite, $Na_{15}(Ca_3Mn_3)(Na_2Fe)Zr_3Si_{26}O_{72}(OH)_3\cdot H_2O$, a new eudialyte-group mineral from the Lovozero alkaline massif, Kola Peninsula. *The Canadian Mineralogist*, **58**, 421-436. DOI: 10.3749/canmin.2000006.

Corongiu G., Kelterbaum R., Kochanski E. (1995) Theoretical Studies of $H^+(H_2O)_5$. *Journal of Physical Chemistry*, **99**, 8038–8044. DOI:10.1021/J100020A029.

Headrick J.M., Bopp J.C., Johnson M.A. (2004) Predissociation spectroscopy of the argon-solvated $H_5O_2^+$ "Zundel" cation in the 1000 – 1900 cm^{-1} region. *Journal of Chemical Physics*, **121**, 11523–11526.

Johnsen, O., Ferraris, G., Gault, R.A., Grice, J.D., Kampf, A.R., Pekov, I.V. (2003) Nomenclature of eudialyte-group minerals. *Canadian Mineralogist*, **41**, 785–794.

Kim J., Schmitt U.W., Gruetzmacher J.A., Voth G.A., Scherer N.E. (2002) The vibrational spectrum of the hydrated proton: Comparison of experiment, simulation, and normal mode analysis. *Journal of Chemical Physics*, **116**, 737–746.

Khomyakov A.P., Nechelyustov G.N., Rastsvetaeva R.K. (2007) Aqualite, $(H_3O)_8(Na,K,Sr)_5Ca_6Zr_3Si_{26}O_{66}(OH)_9Cl$, a new eudialyte-group mineral from Inagli alkaline massif (Sakha-Yakutia, Russia), and the problem of oxonium in hydrated eudialytes. *Zapiski Rossiiskogo Mineralogicheskogo Obshchestva* (*Proceedings of the Russian Mineralogical Society*), **136**(2), 39-55 (in Russian).

https://doi.org/10.1180/mgm.2022.136 Published online by Cambridge University Press

Komatsuzaki T. and Ohmine I. (1994) Energetics of proton transfer in liquid water. I. Ab initio study for origin of many-body interaction and potential energy surfaces. *Chemical Physics*, **180**, 239–269. DOI:10.1016/0301-0104(93)e0424-t.

Laria D., Martí J., Guàrdia E. (2004) Protons in supercritical water: A multistage empirical valence bond study. *Journal of American Chemical Society*, **126**, 2125–2134. DOI: 10.1021/ja0373418.

Libowitzky E. (1999) Correlation of O–H stretching frequencies and O–H···O hydrogen bond lengths in minerals. *Monatshefte für Chemie*, **130**, 1047–1059.

Lykova I.S., Pekov I.V., Chukanov N.V., Belakovskiy D.I., Yapaskurt V.O., Zubkova N.V., Britvin S.N., Giester G. (2016) Calciomurmanite, $(Na,\square)_2Ca(Ti,Mg,Nb)_4[Si_2O_7]_2O_2(OH,O)_2(H_2O)_4$, a new mineral from the Lovozero and Khibiny alkaline complexes, Kola Peninsula, Russia. *European Journal of Mineralogy*, 24, 835–845. DOI: 10.1127/ejm/2016/0028-2550.

Mandarino J.A. (1981) The Gladstone-Dale relationship. IV. The compatibility concept and its application. *The Canadian Mineralogist*, **41**, 989–1002.

McClellan A.L. and Pimentel G.C. (1960) Hydrogen bond. W.H.Freeman & Co Ltd, California Univ. 475 pp.

Ortega I.K., Escribano R., Herrero V.J., Maté B., Moreno M.A. (2005) The structure and vibration frequencies of crystalline HCl trihydrate. *Journal of Molecular Structure*, **742**, 147–152. DOI: 10.1016/j.molstruc.2005.01.005.

Oxford Diffraction (2009) CrysAlisPro. Oxford Diffraction Ltd, Abingdon, Oxfordshire, UK.

Paddison S.J. and Elliott J.A. (2005): Molecular modeling of the short-side-chain perfluorosulfonic acid membrane. *Journal of Physical Chemistry A*, **109**, 7583–7593, https://doi.org/10.1021/jp0524734

Petříček V, Dušek M, Palatinus L (2006) Jana2006. Structure determination software programs. Institute of Physics, Praha, Czech Republic.

https://doi.org/10.1180/mgm.2022.136 Published online by Cambridge University Press

Prince E (Ed.) (2004) International Tables for Crystallography, Volume C: Mathematical, Physical and Chemical Tables, 3rd Edition. Kluwer Academic Publishers, Dordrecht.

Rastsvetaeva R.K., Chukanov N.V., Aksenov S.M. (2012) Eudialyte-group minerals. Nizhny Novgorod State University, Nizhny Novgorod. 230 pp. (in Russian).

Rastsvetaeva R.K., Chukanov N.V., Pekov I.V., Vigasina M.F. (2022) Crystal-chemical feastures of a cation-ordered potassium analogue of aqualite fron the Kovdor massif, Kola Peninsula. *Zapiski Rossiiskogo Mineralogicheskogo Obshchestva* (*Proceedings of the Russian Mineralogical Society*), **151**(4), 81–101 (in Russian). DOI: 10.31857/S0869605522040074.

Sobolewski A.L. and Domcke W. (2002a) Hydrated hydronium: a cluster moder or solvated electron? *Physical Chemistry Chemical Physics*, **4**, 4–10. DOI: 10.1039/b107373g.

Sobolewski A.L. and Domcke W. (2002b) *Ab initio* investigation of the structure and spectroscopy of hydronium-water clusters. *Journal of Physical Chemistry A*, **106**, 4158-4167.

Vener M.V. and Librovich N.B. (2009) The structure and vibrational spectra of proton hydrates: $H_5O_2^+$ as a simplest stable ion. *International Reviews in Physical Chemistry*, **28**, 407–434. DOI: 10.1080/01442350903079955.

Vyas N.K., Sakore T.D., Biswas A.B. (1978) The structure of 4-methyl-5-sulphosalicylic acid tetrahydrate. *Acta Crystallographica B*, **34**, 3486–3488. https://doi.org/10.1107/S0567740878011413

https://doi.org/10.1180/mgm.2022.136 Published online by Cambridge University Press

List of Figures:

FIG. 1. A fragment of the holotype specimen with red to reddish-orange selsurtite grains emnedded in the aegirine-feldspar rock (a) and selsurtite crystal (brownish-red on the left) in association with lorenzenite (dark brown on the right) (b). The FOV widths are 15 mm (a) and 4 cm (b).

FIG. 2. SEM (BSE) image of a polished section of a fragment of selsurtite (Ssu) holotype specimen in a rock composed of aegirine (Aeg), orthoclase (Or) and albite (Ab) with accessory lorenzenite (Lrz) (a) and enlarged fragment of this image showing relics of sergevanite (Sgv) with the empirical formula $Na_{9.47}(H_3O)_xK_{0.16}Sr_{0.47}(Ca_{3.48}Mn_{2.01}Fe_{0.32}Ln_{0.19})(Na_{2.05}Fe_{0.56}Zr_{0.39})(Zr_{2.84}Ti_{0.09}Hf_{0.07})(Si_{25.58}Nb_{0.42})Cl_{1.00}(SO_4)_{0.04}(O,OH)_y \cdot nH_2O$ in the selsurtite crystal (b).

FIG. 3. Powder infrared absorption spectra of (*a*) selsurtite and (*b*) sergevanite holotype sample with the crystal-chemical formula $^{N1\text{-}4}(Na_{10.5}K_{0.9}REE_{0.6})\ ^{N5}[(H_3O,H_2O)_{2.25}Na_{0.75}]\ ^{M11}Ca_3\ ^{M12}(Mn_{1.8}Ca_{1.2})\ ^{M2}(Na_{2.4}Fe^{2+}_{0.6})\ ^{M3}(Si_{0.5}Ti_{0.45}Nb_{0.05})\ ^{M4}Si\ ^{Z}(Zr_{2.7}Nb_{0.3})\ [Si_3O_9]_2\ [Si_9O_{27}]_2\ (OH)_3\ (SO_4)_{0.3}\ ^{X1}[(H_2O)_{0.8}Cl_{0.2}]$. The spectra are offset for comparison.

FIG. 4. Raman spectrum of selsurtite.

FIG. 5. Raman spectra of (*a*) potassium analogue of aqualite $(H_3O)_8Na_5K_2Zr_3Ca_6[Si_{24}O_{69}(OH)_3][Si_2]Mn(OH)_2Cl \cdot 2H_2O$ from the Kovdor ultrabasic-alkaline-carbonatite complex, Kola Peninsula, Russia (Rastsvetaeva *et al*., 2022), (*b*) "potassium-oxonium eudialyte" with the empirical formula $(H_3O)_x(Na_{3.3}K_{2.5}Sr_{0.6})Ca_{6.4}Mn_{0.15}Fe_{1.3}Zr_{2.8}Ti_{0.2}Nb_{0.15}Si_{25.85}Cl_{1.7}(O,OH)_x \cdot nH_2O$ ($x \approx 8$) from the Kukisvumchorr mountain, Khibiny alkaline massif, Kola Peninsula (Rastsvetaeva *et al*., 2012), and (*c*) common accessory eudialyte $Na_{15}Ca_6Fe^{2+}_3Zr_3Si_{26}O_{72}(O,OH,H_2O)_3Cl_2$ from the Alluaiv mountain, Lovozero alkaline massif, Kola Peninsula.

FIG. 6. distribution of Na and Zr over the *M*2-sites in the crystal structure of selsurtite.

https://doi.org/10.1180/mgm.2022.136 Published online by Cambridge University Press

FIG. 7. The dependence of the wavenumber shift of O–H stretching vibrations relative to the value of 3750 cm^{-1} (accepted for non-bonded OH group) on the O···O distances for hydrogen bonds in crystals drawn using data from McClellan & Pimentel (1960).

https://doi.org/10.1180/mgm.2022.136 Published online by Cambridge University Press

Table 1. Crystal data, data collection information and structure refinement details for selsurtite.

Crystal data	
Simplified formula	$(H_3O)_{12}Na_3(Mn_3Ca_3)(Na_2Fe)Zr_3$ □$Si[Si_{24}O_{69}(OH)_3](OH)Cl\cdot H_2O$
Formula weight	2868.5*
Crystal system	Trigonal
Space group	*R*3 (#146)
Lattice Parameters *a* (Å) *c* (Å) *V* (Å^3)	 14.1475(7) 30.3609(12) 5262.65(7)
Z	3
Crystal size (mm)	0.09×0.11×0.11
Crystal form	Anhedral grain
Crystal color	Reddish
Data Collection	
Diffractometer	Rigaku XtaLAB Synergy
Radiation; λ	MoK_α; 0.71073
Absorption coefficient, μ (mm^{-1})	2.372
F (000)	4194
Data range θ (º); *h*, *k*, *l*	3.39 – 33.54; $-19 < h < 20$, $-17 < k < 20$, $-46 < l < 31$
No. of measured reflections	10863
Total reflections (N_{tot}) / unique(N_{ref})	2752 / 3527
R_{int} (%)	2.73
Criterion for observed reflections	$I > 3\sigma(I)$
Refinement	
Refinement on	Full-matrix least squares on *F*
Weight scheme	$1/(\sigma^2\|F\|+ 0.0025F^2)$
R_1 / wR_2	4.84 / 7.15
No. of refinement parameters (N_{par})	424
N_{ref}/N_{par}	12.35
GOF (Goodness of fit)	1.14
Min./max. residual *e* density, (*e* Å^{-3})	–1.11 / 1.14

*Note: The weight of the refined formula is close to the empirical formula weight of 2869.8.

https://doi.org/10.1180/mgm.2022.136 Published online by Cambridge University Press

Table 2. Chemical composition of selsurtite.

Constituent	Wt%	Range	Standard deviation	Standard
Na_2O	6.48	5.21 – 7.50	0.75	Albite
K_2O	0.27	0.09 – 0.77	0.20	Orthoclase
MgO	0.10	bdl – 0.42	0.13	MgO
CaO	6.83	6.12 – 7.30	0.39	Wollastonite
MnO	4.73	3.98 – 5.48	0.52	Mn
FeO	1.18	0.81 – 1.93	0.29	Fe
SrO*	1.88	1.43 – 2.63	0.37	SrF_2
La_2O_3	0.57	0.13 – 1.15	0.35	$LaPO_4$
Ce_2O_3	1.07	0.44 – 1.71	0.38	$CePO_4$
Pr_2O_3	0.20	bdl – 0.38	0.18	$PrPO_4$
Nd_2O_3	0.44	bdl – 1.44	0.42	$NdPO_4$
Al_2O_3	0.29	0.02 – 0.62	0.19	Albite
SiO_2	50.81	49.60 – 51.59	0.66	SiO_2
ZrO_2	13.50	12.01 – 15.08	0.85	Zr
HfO_2	0.45	0.19 – 0.68	0.23	Hf
TiO_2	0.61	0.44 – 0.93	0.17	Ti
Nb_2O_5	1.10	0.73 – 1.54	0.31	Nb
Cl	1.01	0.87 – 1.25	0.11	NaCl
SO_3	0.29	0.10 – 0.47	0.18	FeS_2
H_2O	8.10			
O≡Cl	–0.23			
Total	99.68			

Note: bdl means “below detection limit”.

* WDS-mode analyses for SrO.

** The H_2O content was determined by modified Penfield method

https://doi.org/10.1180/mgm.2022.136 Published online by Cambridge University Press

Table 3. Powder X-ray diffraction data (d in Å) of selsurtite.

I_{obs}	d_{obs}	I_{calc}*	d_{calc}**	$h\ k\ l$	I_{obs}	d_{obs}	I_{calc}*	d_{calc}**	$h\ k\ l$	I_{obs}	d_{obs}	I_{calc}*	d_{calc}**	$h\ k\ l$
56	11.38	66	11.362	101	7	2.535	4	2.539	2.1.10	31	1.773	7	1.774	-4.6.11
5	10.14	2	10.120	003			1	2.532	-348			9	1.770	0.4.14
59	7.08	100	7.074	110			7	2.530	0.0.12			16	1.768	440
29	6.46	41	6.452	104	14	2.446	8	2.442	051	8	1.752	4	1.757	-2.4.15
34	6.01	10	6.005	021			5	2.441	-249			4	1.747	-381
4	5.80	1	5.798	113	9	2.387	9	2.384	048			1	1.747	609
36	5.69	38	5.681	202	8	2.366	4	2.364	-456	5	1.719	4	1.717	2.3.14
13	5.45	13	5.441	015	13	2.313	11	2.309	241	4	1.700	1	1.706	354
7	5.06	6	5.060	006	6	2.297	1	2.296	-363			2	1.696	-681
3	4.785	2	4.767	024			2	2.294	1.0.13	7	1.692	6	1.689	-282
5	4.582	2	4.578	-231			3	2.289	422	8	1.673	10	1.669	-486
3	4.430	1	4.429	122	5	2.265	2	2.264	1.3.10	8	1.644	5	1.644	-2.6.13
72	4.318	51	4.313	205			2	2.259	-258			3	1.641	1.1.18
23	4.105	16	4.116	116	7	2.180	5	2.178	152	10	1.616	2	1.614	-4.5.15
		5	4.089	107	24	2.161	6	2.163	425			9	1.613	4.0.16
		4	4.084	300			17	2.156	4.0.10	5	1.593	3	1.591	-1.7.10
19	3.958	19	3.953	214	12	2.144	6	2.142	3.1.11	8	1.585	1	1.589	0.6.12
36	3.793	28	3.787	303			1	2.137	-366			2	1.583	4.2.14
5	3.688	4	3.682	125			3	2.135	0.1.14			4	1.582	-687
17	3.630	13	3.625	018	6	2.118	5	2.114	-564	5	1.576	6	1.573	-3.5.16
72	3.544	24	3.540	027	4	2.099	2	2.095	149	7	1.548	3	1.550	-2.7.12
		13	3.537	220	9	2.065	4	2.065	3.2.10			4	1.545	-1.6.14
35	3.382	25	3.377	131			4	2.058	-2.4.12			3	1.544	630
		3	3.373	009	5	2.012	4	2.010	-471	6	1.527	1	1.526	-393
21	3.336	10	3.339	-243	5	2.006	3	2.002	603			3	1.525	-4.7.13
25	3.230	22	3.226	208			1	2.000	342			3	1.524	802
30	3.175	11	3.178	036	12	1.980	11	1.977	-468	7	1.481	2	1.483	-6.8.10
		14	3.166	217	4	1.950	2	1.947	-474			5	1.478	-5.8.11
17	3.048	12	3.045	-129			2	1.946	-1.2.15	2	1.471	1	1.473	2.0.20
100	2.970	69	2.965	315	3	1.934	2	1.933	-369			1	1.469	274
17	2.903	13	2.899	-246	2	1.915	1	1.912	-375	4	1.452	1	1.453	725
100	2.844	89	2.840	404	8	1.897	9	1.894	066			1	1.450	-498
2	2.770	1	2.764	-252	3	1.864	3	1.865	-171			3	1.449	-4.8.12
12	2.724	11	2.720	0.2.10	9	1.837	4	1.841	2.4.10	2	1.441	2	1.443	-1.3.20
24	2.679	16	2.675	137			6	1.838	1.4.12			2	1.438	0.6.15
		9	2.674	140	3	1.817	1	1.814	-174	2	1.421	3	1.420	808
13	2.640	13	2.636	324			1	1.814	0.3.15	3	1.404	2	1.404	-4.10.1
21	2.604	21	2.601	039	8	1.785	1	1.786	615			1	1.401	-399
							6	1.782	-5.6.10					

*For the calculated pattern, only reflections with intensities ≥1 are given.

**For the unit-cell parameters calculated from single-crystal data.

https://doi.org/10.1180/mgm.2022.136 Published online by Cambridge University Press

Table 4. Atom coordinates (*x, y, z*), atomic displacement parameters (U, Å^2), site multiplicities (*Mult*), and site occupancies (s.o.f.) in the structure of selsurtite

Site	*x*	*y*	*z*	U_{eq}/ U_{iso}*	*Mult*	s.o.f.
Z	0.8337(1)	0.6663(1)	0.1651(1)	0.0197(2)	9	$Zr_{0.977}Hf_{0.023}$
*M*1(1)	0.9297(2)	0.5970(2)	0.3314(11)	0.0272(6)	9	$Mn_{0.607}Ca_{0.327}REE_{0.066}$
*M*1(2)	0.6670(2)	0.5923(2)	0.3315(11)	0.0327(7)	9	$Ca_{0.9}Mn_{0.063}REE_{0.037}$
Si1	0.9299(2)	0.8581(2)	0.07868(10)	0.0257(10)	9	Si
Si2	0.0815(3)	0.5401(2)	0.25542(11)	0.0295(11)	9	Si
Si3	0.2069(2)	0.7948(2)	0.07497(10)	0.0267(10)	9	Si
Si4	0.9912(2)	0.6037(2)	0.09555(9)	0.0246(9)	9	Si
Si5	0.3958(2)	0.0085(2)	0.09540(9)	0.0219(9)	9	Si
Si6	0.0538(2)	0.7293(2)	0.23502(9)	0.0249(9)	9	Si
Si7	0.0538(2)	0.3246(2)	0.23522(9)	0.0237(9)	9	Si
Si8	0.7371(2)	0.4725(2)	0.25112(9)	0.0245(9)	9	Si
O1	0.0173(7)	0.5083(6)	0.1041(5)	0.057(4)	9	O
O2	0.8772(6)	0.9387(6)	0.0777(4)	0.044(3)	9	O
O3	0.1797(5)	0.8195(6)	0.2200(2)	0.031(2)	9	O
O4	0.2790(6)	0.9002(6)	0.1035(3)	0.043(3)	9	O
O5	0.2092(10)	0.6055(11)	0.2587(4)	0.066(5)	9	O
O6	0.0984(6)	0.7206(6)	0.1035(3)	0.039(3)	9	O
O7	0.8885(10)	0.7764(10)	0.0399(3)	0.063(6)	9	O
O8	0.1782(7)	0.8230(7)	0.0280(2)	0.040(4)	9	O
O9	0.0308(10)	0.5152(9)	0.3044(4)	0.058(5)	9	O
O10	0.0404(7)	0.7404(7)	0.2889(3)	0.040(3)	9	O
O11	0.0378(7)	0.4305(6)	0.2241(3)	0.036(3)	9	O
O12	0.0406(7)	0.2989(7)	0.2876(3)	0.040(3)	9	O
O13	0.9706(7)	0.2275(6)	0.2023(3)	0.042(3)	9	O
O14	0.0373(6)	0.6077(6)	0.2243(2)	0.032(3)	9	O
O15	0.8994(7)	0.5866(7)	0.1263(3)	0.036(3)	9	O
O16	0.9548(10)	0.6020(8)	0.0455(3)	0.066(4)	9	O
O17	0.4147(6)	0.1053(6)	0.1278(3)	0.034(3)	9	O
O18	0.8964(11)	0.8026(7)	0.1245(3)	0.059(5)	9	O
O19	0.9724(7)	0.7398(8)	0.2043(4)	0.047(4)	9	O
O20	0.2714(6)	0.7270(7)	0.0740(4)	0.052(4)	9	O

https://doi.org/10.1180/mgm.2022.136 Published online by Cambridge University Press

O21	0.7629(7)	0.5303(7)	0.2038(2)	0.040(3)	9	O
O22	0.3973(8)	0.0435(9)	0.0462(3)	0.062(4)	9	O
O23	0.7916(7)	0.3958(7)	0.2546(3)	0.039(3)	9	O
O24	0.7761(9)	0.5531(8)	0.2932(4)	0.060(4)	9	O
*M*2a	0.1776(5)	0.8232(5)	0.332(1)	0.0443(18)	9	$Zr_{0.127}Fe_{0.123}$
*M*2b	0.1520(6)	0.8482(5)	0.333(1)	0.046(3)	9	$Na_{0.707}Fe_{0.043}$
*M*3a	0.3333	0.6667	0.0917(1)	0.027(3)*	3	$Si_{0.261}$
OH^{M3a}	0.3333	0.6667	0.1512(11)	0.17(10)	3	$(OH)_{0.261}$
*M*3b	0.3333	0.6667	0.0455(11)	0.064(3)	3	$Nb_{0.3}$
OH^{M3b}	0.0773(15)	0.9158(14)	0.3354(6)	0.081(8)	9	$(OH)_{0.3}(H_2O)_{0.407}$
*M*4a	0.3333	0.6667	0.3010(11)	0.0142(16)	3	$Ti_{0.23}$
OH^{M4a}	0.4616(19)	0.7327(19)	0.3354(8)	0.024(4)*	9	$(OH)_{0.23}(H_2O)_{0.02}$
*M*4b	0.3333	0.6667	0.2394(2)	0.097(15)	3	$Si_{0.3}$
OH^{M4b}	0.3333	0.6667	0.1867(11)	0.029(6)*	3	$(OH)_{0.3}$
*N*1	0.7821(5)	0.8915(5)	0.1516(3)	0.0275(18)	9	$(H3O)_{0.8}Na_{0.2}$
*N*2	0.8654(8)	0.4331(5)	0.1725(2)	0.055(4)	9	$(H_3O)_{0.7}Na_{0.3}$
*N*3	0.9018(3)	0.8022(3)	0.2847(11)	0.0392(14)	9	$Na_{0.6}(H_3O)_{0.28}Sr_{0.12}$
*N*4	0.7716(4)	0.5419(5)	0.0432(11)	0.036(2)	9	$(H_3O)_{0.3}Na_{0.233}K_{0.06}$
*X*1a	0	0	0.2305(11)	0.073(2)	3	$Cl_{0.81}$
*X*1b	0	0	0.1965(11)	0.098(14)*	3	$S_{0.12}F_{0.07}$
*X*2	0.6667	0.3333	0.1271(11)	0.014(7)*	3	$(H_2O)_{0.16}$

https://doi.org/10.1180/mgm.2022.136 Published online by Cambridge University Press

Table 5. Selected interatomic distances (Å) in the structure of selsurtite.

Bond		Distance	Bond		Distance
Z	O13	2.036(11)	*M*1(1)	O16	2.214(24)
	O21	2.040(8)		O10	2.248(21)
	O19	2.075(9)		O24	2.260(21)
	O18	2.077(9)		O7	2.308(23)
	O17	2.092(8)		O8	2.358(17)
	O15	2.138(11)		O9	2.390(20)
Mean		2.076	*Mean*		2.296
Si1	O7	1.545(11)	*M*1(2)	O24	2.212(23)
	O18	1.550(9)		O22	2.269(25)
	O2	1.624(7)		O7	2.274(21)
	O2	1.646(11)		O12	2.337(22)
Mean		1.591		O8	2.349(15)
Si2	O5	1.568(13)		O9	2.388(17)
	O9	1.612(13)	*Mean*		2.304
	O11	1.653(9)	*M*2a	O10	2.131(22)
	O14	1.672(10)		O12	2.143(23)
Mean		1.626		O16	2.298(23)
Si3	O4	1.579(8)		O22	2.298(23)
	O8	1.587(8)		OH^{M3b}	2.367(27)
	O6	1.612(8)	*Mean*		2.246
	O20	1.621(12)		*M*2b	0.622(14)
Mean		1.600	*M*2b	O10	2.056(24)
Si4	O15	1.517(10)		O12	2.073(24)
	O1	1.589(11)		O16	2.421(22)
	O16	1.601(10)		O22	2.422(22)
	O6	1.608(6)		OH^{M4a}	2.875(34)
Mean		1.581	*Mean*		2.369
Si5	O22	1.571(10)	*N*1	O2	2.527(13)
	O1	1.584(12)		O13	2.553(12)
	O17	1.596(9)		O19	2.592(14)
	O4	1.615(6)		O18	2.628(18)
Mean		1.592		O3	2.713(8)
Si6	O19	1.546(12)		O18	2.737(10)
	O14	1.649(9)		O6	2.755(12)
	O3	1.654(6)		O4	2.764(9)
	O10	1.663(9)	*Mean*		2.650
Mean		1.628		*X*1b	2.998(16)
Si7	O12	1.621(9)	*N*2	O17	2.409(13)
	O13	1.629(8)		O15	2.423(12)

https://doi.org/10.1180/mgm.2022.136 Published online by Cambridge University Press

	O11	1.658(11)		O21	2.583(10)
	O3	1.667(7)		O21	2.625(16)
Mean		1.644		O23	2.652(11)
Si8	O21	1.602(7)		O1	2.789(15)
	O24	1.615(12)		O14	2.912(9)
	O23	1.619(13)		O11	2.915(15)
	O23	1.638(9)	*Mean*		2.664
Mean		1.619		*X*2	2.798(19)
*M*3a	O20 ×3	1.592(16)	*N*3	O10	2.518(13)
	OH^{M3a}	1.807(47)		O12	2.524(11)
Mean		1.646		OH^{M3b}	2.670(26)
	*M*3b	1.403(47)		O8	2.712(30)
*M*3b	O20 ×3	1.730(20)		OH^{M3b}	2.758(29)
	OH^{M3b} ×3	2.378(26)		O19	2.936(31)
Mean		2.054		O13	2.962(29)
*M*4a	OH^{M4a} ×3	1.887(36)	*Mean*		2.726
	O5 ×3	1.991(25)		*X*1a	2.929(27)
Mean		1.939	*N*4	O16	2.290(15)
	*M*4b	1.871(33)		O22	2.328(16)
*M*4b	OH^{M4b}	1.600(20)		O9	2.474(32)
	O5 ×3	1.630(12)		O7	2.875(14)
Mean		1.623		O15	2.982(30)
				O17	2.999(30)
			Mean		2.631
				OH^{M4a}	2.530(35)
				OH^{M4a}	2.586(26)

https://doi.org/10.1180/mgm.2022.136 Published online by Cambridge University Press

Table 6. The shortest O···O distances for hydrogen bonds in selsurtite estimated from the Raman spectrum using $\nu/d_{O\cdots O}$ correlations [$d_{O\cdots O}(calc)$] and determined as a result of the crystal structure refinement [$d_{O\cdots O}(ref)$].

Wavenumber, ν (cm^{-1})	$d_{O\cdots O}(calc)$ (Å) (McClellan and Pimentel, 1960)	$d_{O\cdots O}(calc)$ (Å) (Libowitzky, 1999)	$d_{O\cdots O}(ref)$ (Å) / O sites (this work)
1073	-	2.46	2.290 / *N*4···O16
1420	2.32*	2.48	2.328 / *N*4···O16
1507	2.34*	2.48	2.409 / *N*2···O17
1725	2.39*	2.50	2.423 / *N*2···O15
1877	2.41	2.51	2.474 / *N*4···O9
2040	2.46	2.52	2.518 / *N*3···O10 2.524 / *N*3···O12
2405	2.53	2.56	2.527 / *N*1···O2
2427	2.54	2.56	2.530 / *N*4···OH^{M4a}
2520	2.57	2.57	2.553 / *N*1···O13
2575	2.58	2.57	2.583 / *N*2···O21
2811	2.62	2.61	2.586 / *N*4···OH^{M4a}
3120	2.69	2.68	2.592 / *N*1···O19 2.670 / *N*3···OH^{M3b}

* Extrapolated values.

https://doi.org/10.1180/mgm.2022.136 Published online by Cambridge University Press

Table 7. Comparative data for selsurtite and other Na-deficient hydrated eudialyte-group minerals.

Mineral	**Selsurtite**	**Ilyukhinite**	**Aqualite**	**Ikranite**
Formula	$(H_3O)_{12}Na_3(Ca_3Mn_3)(Na_2Fe)Zr_3$ $\square Si[Si_{24}O_{69}(OH)_3](OH)Cl\cdot H_2O$	$(H_3O,Na)_{14}Ca_6Mn_2Zr_3$ $Si_{26}O_{72}(OH)_2\cdot 3H_2O$	$(H_3O)_8Na_4SrCa_6Zr_3$ $Si_{26}O_{66}(OH)_9Cl$	$(Na,H_3O)_{15}Ca_6Fe^{3+}{}_2Zr_3$ $\square_2Si_{24}O_{68}(OH)_4Cl\cdot 3H_2O$
Crystal system **Space group**	Trigonal *R*3	Trigonal *R*3*m*	Trigonal *R*3	Trigonal *R*3*m*
***a*, Å**	14.1475	14.1695	14.078	14.167
***c*, Å**	30.3609	31.026	31.24	30.081
***V*, Å^3**	5262.65	5394.7	5362	5229
Z	3	3	3	3
Strong lines of the powder X-ray diffraction pattern: d, Å (I, %)	11.38 (56) 7.08 (59) 5.69 (36) 4.318 (72) 3.793 (36) 3.544 (72) 2.970 (100) 2.844 (100)	11.44 (82) 7.09 (70) 6.02 (44) 4.371 (89) 3.805 (47) 3.376 (41) 2.985 (100) 2.852 (92)	11.43(39) 10.50(44) 7.06(42) 6.63(43) 4.39(100) 3.624(41) 2.987(100) 2.850(79)	6.41 (41) 4.30 (91) 4.09 (36) 3.521 (57) 3.205 (44) 2.963 (92) 2.841 (100)
Optical data	Uniaxial (–) ω = 1.598 ε = 1.595	Uniaxial (–) ω = 1.585 ε = 1.584	Uniaxial (+) ω = 1.569 ε = 1.571	Uniaxial (+) ω = 1.612 ε = 1.615
Density, g·cm^{-3}	2.73 (meas.) 2.722 (calc.)	2.67 (meas.) 2.703 (calc.)	2.58 (meas.) 2.66 (calc.)	2.82 (meas.) 2.83 (calc.)
Dominant components at the key sites				
***N*1–*N*5**	H_3O	H_3O	H_3O	Na
***M*1**	Mn^{2+}+Ca	Ca	Ca+Ca	Ca
***M*2**	Na	Mn^{2+}	□	Fe^{3+}
***M*3**	□	Si	Si	□
***M*4**	Si	Si	Si	□
References	This work	Chukanov *et al*., 2017	Khomyakov *et al*., 2007	Chukanov *et al*., 2003

https://doi.org/10.1180/mgm.2022.136 Published online by Cambridge University Press